

## Radiative transfer based scaling of LAI retrievals from reflectance data of different resolutions

Yuhong Tian<sup>a,b,\*</sup>, Yujie Wang<sup>a</sup>, Yu Zhang<sup>a</sup>, Yuri Knyazikhin<sup>a</sup>,  
Jan Bogaert<sup>a,c</sup>, Ranga B. Myneni<sup>a</sup>

<sup>a</sup>Department of Geography, Boston University, Boston, MA 02215, USA

<sup>b</sup>School of Earth and Atmospheric Sciences, Georgia Institute of Technology, Atlanta, GA 30332, USA

<sup>c</sup>Department of Biology, University of Antwerp, B-2610 Wilrijk, Belgium

Received 13 April 2001; received in revised form 31 May 2002; accepted 5 June 2002

### Abstract

The problem of how the scale, or spatial resolution, of reflectance data impacts retrievals of vegetation leaf area index (LAI) is addressed in this article. We define the goal of scaling as the process by which it is established that LAI values derived from coarse resolution sensor data equal the arithmetic average of values derived independently from fine resolution sensor data. The increasing probability of land cover mixtures with decreasing resolution is defined as heterogeneity, which is a key concept in scaling studies. The effect of pixel heterogeneity on spectral reflectances and LAI retrievals is investigated with 1-km Advanced Very High Resolution Radiometer (AVHRR) data aggregated to different coarse spatial resolutions. It is shown that LAI retrieval errors at coarse resolution are inversely related to the proportion of the dominant land cover in such pixel. Further, large errors in LAI retrievals are incurred when forests are minority biomes in non-forest pixels compared to when forest biomes are mixed with one another, and vice versa. A physically based scaling with explicit spatial resolution-dependent radiative transfer formulation is developed. The successful application of this theory to scaling LAI retrievals from AVHRR data of different resolutions is demonstrated. These principles underlie our approach to the production and validation of LAI product from the Moderate Resolution Imaging Spectroradiometer (MODIS) and the Multi-angle Imaging Spectroradiometer (MISR) aboard the TERRA platform.

© 2002 Elsevier Science Inc. All rights reserved.

### 1. Introduction

Vegetation–atmosphere interactions can be conveniently grouped into biogeophysical (energy and water exchanges) and biogeochemical (carbon and volatile organic compound exchanges) themes (Sellers et al., 1997). Models of these processes, e.g., land surface parameterizations in climate models, are key tools for evaluating the role of vegetation in the context of global climate change and variability (Running et al., 1999). The utility of such models is significantly enhanced when they can be either forced or tested with satellite data products, in view of the coverage, repeatability and consistency of remote sensing products.

One of the key state variables in land surface models is the vegetation green leaf area index (LAI), defined as half the all-sided green leaf area per unit ground area. Vegetation leaf area index governs net radiation and its expenditure (energy balance), net primary production (carbon fixation), evapotranspiration and canopy interception (water budget). As such, there is considerable interest in developing algorithms for the estimation of LAI from satellite measurements of vegetation reflectance (Knyazikhin, Martonchik, Diner, et al., 1998; Knyazikhin, Martonchik, Myneni, et al., 1998), and also to assemble time series of LAI data from the archive of almost two decades of AVHRR data to study interannual global vegetation dynamics (Myneni, Tucker, Asrar, & Keeling, 1998).

Several complicated issues arise when one attempts to assemble a consistent time series of LAI and other biophysical products with data from different instruments. One needs to account for varying radiometric integrity, spectral

\* Corresponding author. School of Earth and Atmospheric Sciences, Georgia Institute of Technology, 221 Bobby Dodd Way, Atlanta, GA 30332, USA. Tel.: +1-404-385-2383; fax: +1-404-385-1510.

E-mail address: ytian@eas.gatech.edu (Y. Tian).

band widths, calibration, geometry of acquisition, etc. A key issue in this context is the possibility of varying spatial resolution of the data from different instruments view angles from the same instrument. This problem may be posed as, how can a time series of a particular biophysical product be developed from data acquired from a series of sensors that have different spatial resolutions?

The issue of spatial resolution, or scale, of image data has been addressed previously, usually depending on the application. For instance, Nelson and Holben (1986) reported that a 1.1 km or higher resolution data are required to identify forested areas. Woodcock and Strahler (1987) argued that a spatial resolution at which the local variance reaches its maximum should be taken as the characteristic scale of scene variation. Other investigators used the concept of entropy to evaluate the feasibility of detecting land cover changes in coarse resolution data (Townshend & Justice, 1988).

We are interested in this article on how the data resolution impacts the retrieval of biophysical parameters, especially LAI. There is conflicting information in the literature as to whether retrieval methods based on the normalized difference vegetation index (NDVI) are spatial resolution dependent or invariant (Hall, Huemmrich, Goetz, Sellers, & Nickeson, 1992; Friedl, 1996; Hu & Islam, 1997). Of special interest are issues related to the use of retrieval methods based on point scale physical models, applied to coarse spatial resolution data, which inevitably contain land cover mixtures (Raffy, 1994; Gregoire & Raffy, 1994; Chen, 1999). In other words, how can a physically based retrieval algorithm be made spatial resolution dependent, such that scaling of the retrieved biophysical product is accomplished when the algorithm is executed on data of multiple resolutions?

The goal of scaling is defined here, as a process by which it is established that values of a certain biophysical product, LAI in this case, derived from coarse resolution sensor data should equal the arithmetic average of values derived independently from fine resolution sensor data. Specifically, we address the problem of LAI retrievals with a 1-km Advanced Very High Resolution Radiometer (AVHRR) data aggregated to different resolutions, in support of our MODIS and MISR LAI and fraction absorbed photosynthetically active radiation (FPAR) algorithm research. MODIS and MISR refer to the Moderate Resolution Imaging Spectroradiometer (MODIS) and Multi-angle Imaging Spectroradiometer (MISR) aboard the TERRA platform launched by National Aeronautics and Space Administration (NASA) in December 1999.

The problem addressed here, that of spatial resolution dependence of algorithms for the retrieval of biophysical variables, arises in two contexts. The first, as previously mentioned, is in the context of assembling time series of biophysical variables with data from sensors of different spatial resolution. The second is in the validation of moderate resolution ( $\sim 1$  km) sensor products such as MODIS

and MISR LAI and FPAR. By validation, we mean specification of the uncertainty in the products in relation to ground truth data. The latter are often collected at resolutions much finer than the products for practical reasons. Therefore, the retrieval algorithms must be spatial resolution dependent so that the products can be validated through scaling, as defined above.

The organization of this paper is as follows. We begin with a brief description of the data and the LAI/FPAR retrieval algorithm used in this study. Then we focus on data analysis, where we demonstrate the relation between land cover heterogeneity and spatial resolution, and the impact of heterogeneity on measured surface reflectances and LAI retrievals. Then we present a physically based technique for scaling with explicit spatial resolution-dependent radiative transfer formulation. We conclude by providing illustrative results that highlight scaling of LAI with the MODIS LAI/FPAR algorithm.

## 2. Data and the LAI algorithm

Land surface reflectances at 1-km resolution from AVHRR over North America for July 1995 are used in this study. The data consisted of channels 1 (580–680 nm) and 2 (725–1100 nm) reflectances, that is, the red and near-infrared bands, respectively. The data processing included radiometric calibration, partial atmospheric corrections, geometric registration and the production of 10-day maximum NDVI value composites (Eidenshink & Faundeen, 2001). A monthly layer based on the maximum NDVI composite of the three 10-day layers was generated for further analysis.

An important ancillary data layer required for our study is the six biome North American land cover map, which was previously developed from a 1-km AVHRR NDVI data of 1995 and 1996, and ancillary data sources (Lotsch, Tian, Friedl, & Myneni, 2001). This map segregates global vegetation into six major biome types depending on vegetation structure and optical properties, and background characteristics (Myneni, Nemani, & Running, 1997). The six biomes include: Grasses and Cereal Crops (biome 1), Shrubs (biome 2), Broadleaf Crops (biome 3), Savannas (biome 4), Broadleaf Forests (biome 5) and Needle Forests (biome 6). Bareland, which is considered as cover type 7 in this study, and water-bodies are also included in this map. The site-based accuracy of this map is 73% (Lotsch et al., 2002). The kappa coefficient ( $\kappa$ ) (Cohen, 1960), which provides a correction for the proportion of chance agreement between reference and test data, is 0.68 (Lotsch et al., 2002). When compared to maps generated from the same data but classified using the International Geosphere Biosphere Program (IGBP) classes (e.g., Loveland et al., 1995; Hansen, Defries, Townshend, & Sohlberg, 2000), the biomes were mapped with  $\sim 5\%$  higher overall accuracy (Lotsch et al., 2002). It should be noted that this classi-

fication accuracy analysis is based on sites that are a priori pure and therefore will not include errors due to sub-pixel mixing.

Of the six biome types, none of them are mixed Broadleaf/Needle Forests. For example, the Natural Resources Canada Land Cover Map of Canada v2.0 indicates 1 377 193 km<sup>2</sup> of Canada covered by mixed forests vs. 953 142 km<sup>2</sup> covered by pure Broadleaf or Needle Forests (Cihlar, Beaubien, Latifovic, & Simard, 1999; Cihlar, Latifovic, Beaubien, Guindon, & Palmer, submitted for publication). This may result in an additional uncertainty in our results.

The structural attributes of these biomes are used to parameterize radiative transfer models (Myneni et al., 1997). Numerical solutions of the three-dimensional radiative transfer equation are used to model the Bi-directional Reflectance Factors (BRF) of the biomes for varying sun-view geometry and canopy/soil patterns (Knyazikhin, Martonchik, Diner, et al., 1998; Knyazikhin, Martonchik, Myneni, et al., 1998). The retrieval of LAI and FPAR is done by comparing the observed and modeled BRFs for a suite of canopy structures and soil realizations. All canopy and soil realizations for which the magnitude of the residuals in the comparison does not exceed uncertainties in observed and modeled BRFs are treated as acceptable solutions. For each acceptable solution, a value of FPAR is also evaluated. The mean values of LAI and FPAR averaged over all acceptable values and their dispersions are taken as the retrievals and their accuracy (Knyazikhin, Martonchik, Diner, et al., 1998; Knyazikhin, Martonchik, Myneni, et al., 1998). This algorithm was prototyped with POLDER, LASUR, Landsat Thematic Mapper (TM), and SeaWiFS data (Tian et al., 2000; Zhang et al., 2000; Wang et al., 2001). The algorithm has been implemented for operational production of LAI and FPAR from MODIS data.

### 3. Data analysis

#### 3.1. Characterizing land cover heterogeneity

We aggregated the 1-km AVHRR reflectance data to 4-, 8-, 16-, 32- and 64-km resolutions. We denote the 1-km pixel as the “sub-pixel” and the aggregated coarse resolution pixels as the “pixel” for the remainder of this paper. We

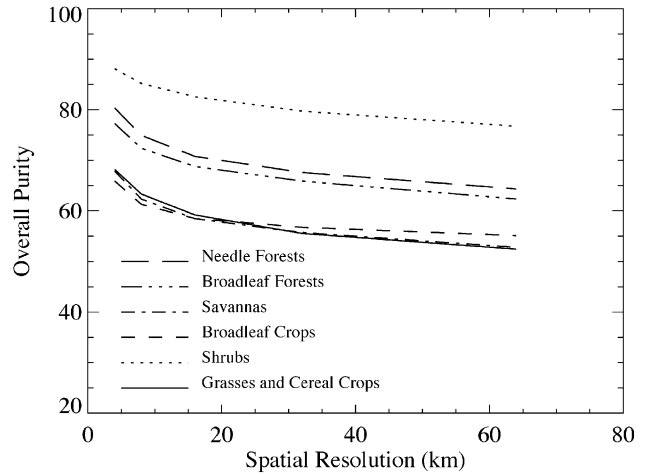


Fig. 1. The overall purity PF(*j*) as a function of spatial resolution.

assume that each sub-pixel contains only one biome type, in view of the 1-km resolution of the biome map. The biome type of a pixel is assigned based on the dominant biome fraction. We did not account for water-bodies because there is no reflectance data for water in the AVHRR data set. Therefore, all aggregations were based on seven land cover types—biomes 1 through 6, and bareland, also denoted as land covers 1 through 7. When a pixel contains only one cover type, it is defined as “homogeneous”. Otherwise, it is heterogeneous. Thus, heterogeneity in this study only indicates that pixels at coarse resolution contain more than one land cover type. It should be noted that our empirical study here only considers scaling error between 1 km and coarser scales and is targeted specifically data sets coarser than 1 km.

We introduce the percentage function (pf) to quantify the heterogeneity of a vegetated pixel. For a pixel,  $pf_l$  ( $l = 1, \dots, 7$ ), is the percent of sub-pixels land cover type  $l$  in the pixel of a given resolution. Note that  $\sum_{l=1}^7 pf_l = 100\%$ . The index  $pf_j$ , which corresponds to the percent occupation of the dominant cover type  $j$  within the pixel, can also be defined as the “purity” or homogeneity of that pixel. Pixels with low  $pf_j$  value are more heterogeneous than those having high values of  $pf_j$ .

The overall percentage function, PF(*j*), is defined as the average of  $pf_j$  over the total number of biome  $j$  pixels in North America at a given resolution. The index PF(*j*) is also called the overall purity of biome  $j$  at that resolution. If PF(*j*) value is higher, on average, biome  $j$  is more homogeneously resolved at that resolution.

The overall percentage functions PF(*j*) at 8-km resolution are given in Table 1. Eight-kilometer resolution pixels denoted as biome 1 have, on average, about 63.32% of sub-pixels containing biome 1. That is, the overall biome 1 purity at 8-km resolution is 63.32%. Shrubs (biome 2) are in general more homogeneously distributed, with about 85.2% of coverage. On the other extreme, Broadleaf Crops (biome

Table 1  
Overall percentage function PF(*j*) at 8-km resolution

Dominant land cover type	Sub-pixel land cover type						
	Biome 1	Biome 2	Biome 3	Biome 4	Biome 5	Biome 6	Bareland
Biome 1	<b>63.32</b>	4.63	5.80	7.12	3.56	11.04	4.54
Biome 2	3.77	<b>85.20</b>	0.50	2.45	1.00	2.59	4.50
Biome 3	12.28	1.92	<b>61.30</b>	9.24	6.09	6.51	2.65
Biome 4	10.62	5.66	5.99	<b>62.34</b>	4.89	6.86	3.64
Biome 5	8.50	2.16	3.97	4.44	<b>72.37</b>	7.33	1.22
Biome 6	9.02	2.96	3.84	3.80	3.52	<b>74.93</b>	1.93

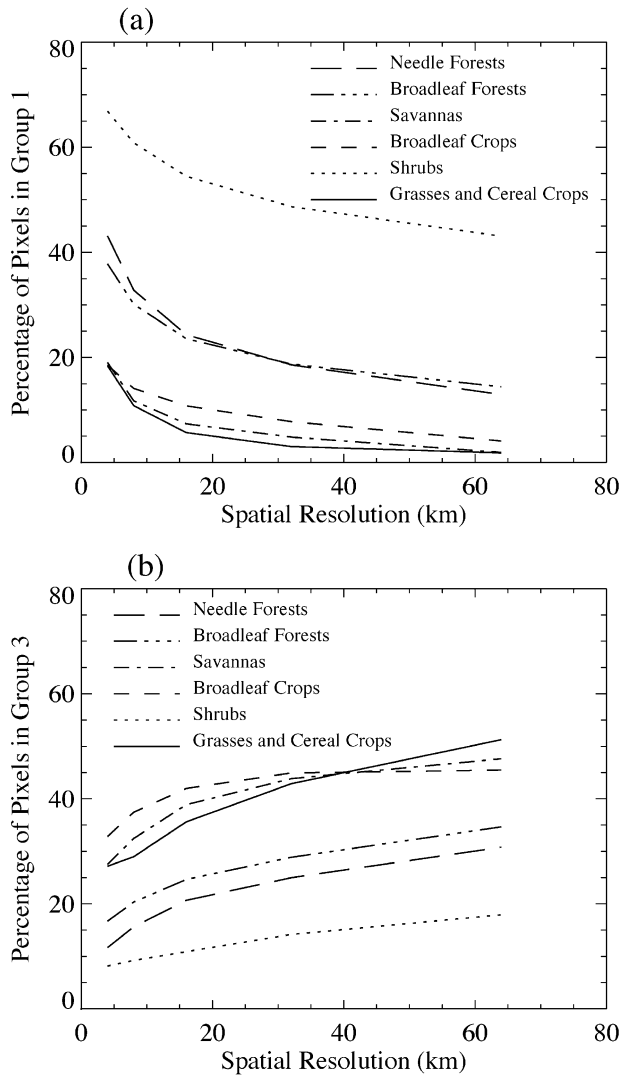


Fig. 2. Percentage of pixels in groups 1 and 3 as a function of spatial resolution: (a) group 1, biome purity  $\geq 90\%$ , (b) group 3, biome purity  $< 50\%$ .

3) are most heterogeneous. The overall purities  $PF(j)$  are shown in Fig. 1 as a function of resolution. The purities decrease with decrease in resolution. Shrubs tend to be most homogeneously resolved at all resolutions followed by Broadleaf and Needle Forests, which is possibly indicative of the natural, that is, undisturbed, state of these biomes.

We divide biome  $j$  pixels into three categories for further analysis. The first group consists of pixels with  $pf_j \geq 90\%$ ; these are assumed to represent homogeneous pixels. The second group consists of nominally heterogeneous pixels with  $50\% \leq pf_j < 90\%$ . The last group contains the rest, that is, heterogeneous pixels with  $pf_j < 50\%$ . In Fig. 2a, we see that the percentage of pixels belonging to group 1 decreases in a nonlinear fashion with decreasing spatial resolution, in all biomes. Similarly, the percentage of pixels belonging to group 3 increases with decreasing spatial resolution (Fig. 2b). This is to be expected in view of increasing mixtures

with increase in pixel area. We conclude that the overall purity  $PF(j)$  decreases with decreasing spatial resolution.

### 3.2. Canopy reflectances and heterogeneity

The data density distribution function was evaluated for each biome as follows: specify a fine grid cell in the

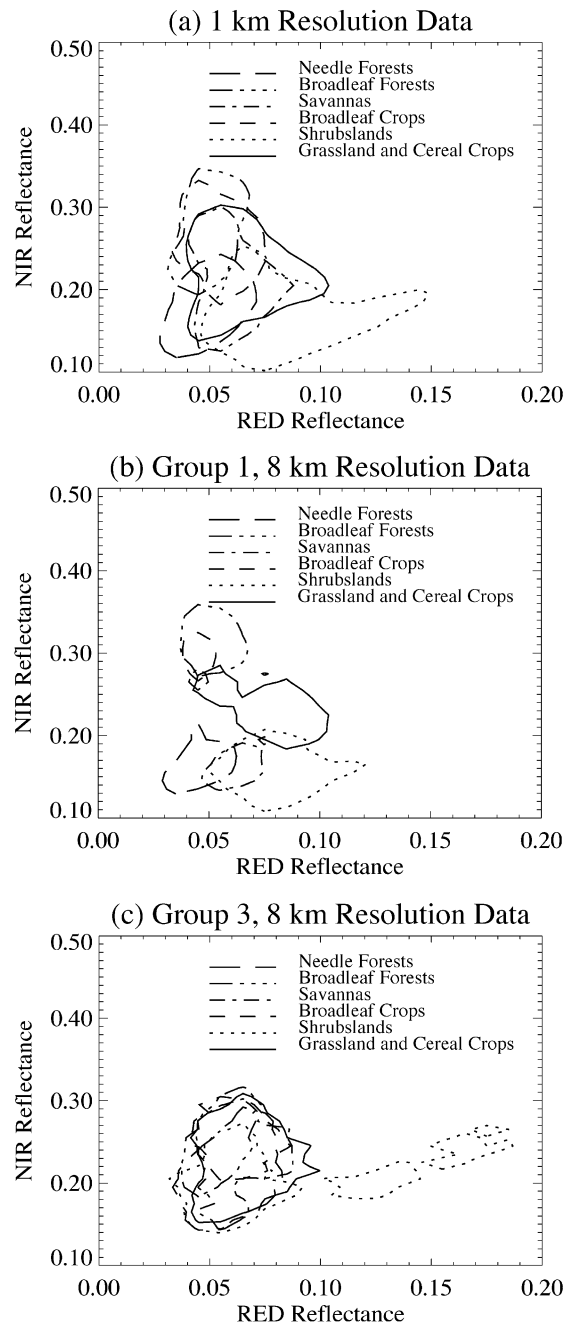


Fig. 3. Contour plot of data density distribution in the spectral space of red and near-infrared (RED–NIR) at (a) 1-km resolution, (b) 8-km resolution from group 1, and (c) 8-km resolution from group 3. Each contour line separates an area in the spectral space with high data density containing 50% of the pixels from a given biome. Groups 1 and 3 represent biome purities  $\geq 90\%$  and  $< 50\%$ , respectively.

spectral space of red and near-infrared reflectances (RED–NIR), count the number of canopy reflectances in this cell, divide this value by the total number of pixels in the entire spectral space (Tian et al., 2000). The location of high density data (50% of all pixels) for each biome in the RED–NIR space is then plotted (Fig. 3). These can be interpreted as the set of pixels representing the most probable patterns of canopy structure for each of the biomes. For instance, Broadleaf Forests and Crops are situated at high near-infrared and low red reflectance locations. Likewise, Needle Forests and Shrubs are located uniquely in the spectral space. The other biomes, however, have considerable overlap. The 50% data density contours at the 1- and 8-km resolution are identical. However, the density contours from pixels with  $pf_j \geq 90\%$ , shown in Fig. 3b, indicate that the biomes have distinct locations in the spectral space. Broadleaf Forests have higher near-infrared reflectance than Broadleaf Crops, and thus, separate better. Likewise, Grasses and Savannas also occupy distinct locations. Thus, it is important to observe homogeneous patches of vegetation types to deduce their reflectance signatures. Also, it is possible to identify such homogeneous patches at any

resolution, provided a finer resolution land cover map is available. This point is further illustrated, in Fig. 3c, where the biome density contours of heterogeneous pixels ( $pf_j < 50\%$ ) are shown to have considerable overlap in the spectral space.

The mean red and near-infrared reflectances of homogeneous and heterogeneous pixels are shown in Fig. 4 as a function of spatial resolution. The reflectance magnitudes of both kinds of pixels do not change much with changing resolution. However, the contrast between the biomes decreases with increasing heterogeneity. This is observed in both spectral bands. It appears cover mixture, rather than spatial resolution, which is critical to determining the spectral signature of a pixel. Also, note that decreasing pixel resolution does not necessarily lead to increasing cover type heterogeneity.

An important issue is the degree of spectral variation in reflectance data from pixels of the same biome type, and how this changes with resolution and pixel heterogeneity. First, we shall assume that the mean red ( $\bar{R}$ ) and near-infrared ( $\bar{N}$ ) reflectance values of homogeneous pixels (group 1;  $pf_j \geq 90\%$ ) represent the correct biome spectral characteristics. Second, we evaluate the average

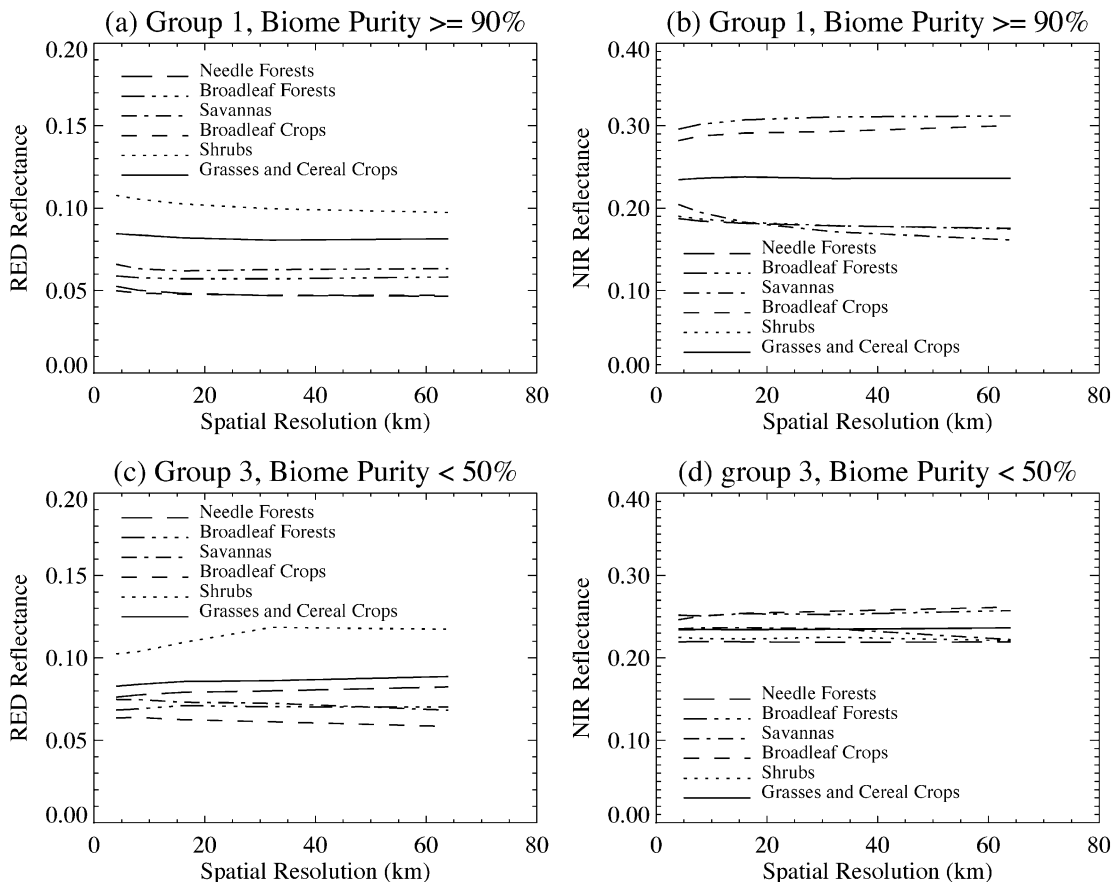


Fig. 4. Mean red (RED) and near-infrared (NIR) reflectance as a function of spatial resolution: (a) group 1 in RED, (b) group 1 in NIR, (c) group 3 in RED, and (d) group 3 in NIR. Groups 1 and 3 represent biome purities  $\geq 90\%$  and  $< 50\%$ , respectively.

distance between pixels from group  $i$  ( $i=1, 2, 3$ ) and point  $(\bar{R}, \bar{N})$ , which can be understood as the deviation from representative biome spectral features,

$$D_i = \frac{1}{K_i} \sum_{k=1}^{K_i} \sqrt{\left(\frac{R_{k,i} - \bar{R}}{\bar{R}}\right)^2 + \left(\frac{N_{k,i} - \bar{N}}{\bar{N}}\right)^2}. \quad (1)$$

Here  $K_i$  is the total number of pixels in group  $i$ ,  $R_{k,i}$  and  $N_{k,i}$  are the red and near-infrared reflectance of the  $k$ th pixels in group  $i$ . We divided by  $\bar{R}$  and  $\bar{N}$  in Eq. (1) in order to equally weight the two spectral bands. The resulting distance values are shown in Fig. 5 as a function of resolution and biome type. The distance values increase with increasing heterogeneity, as expected. Shrubs have a large distance

value compared to other biomes at a given level of homogeneity and resolution, indicating that these are spectrally heterogeneous media. This spectral variation within a biome type can also lead to misclassification if the training data set is not representative of the full range of spectral variations.

### 3.3. LAI retrievals and heterogeneity

Let  $L_t$  denote vegetation LAI values at resolutions 4, 8, 16, 32 and 64 km, obtained by averaging 1-km LAI retrievals. Let  $L_c$  denote LAI retrievals obtained directly from 4-, 8-, 16-, 32- and 64-km surface reflectance data. The discrepancy between  $L_t$  and  $L_c$  defines the response of the LAI retrieval algorithm to heterogeneity of the medium. Therefore, we propose the following to quantify the spatial resolution effect on the algorithm,

$$RDL = |L_t - L_c|/L_t. \quad (2)$$

In the above, RDL denotes LAI error incurred by first averaging reflectances and then performing LAI retrievals. The average value of RDL for a given biome is termed here as the “overall RDL”. Likewise, RDFPAR denotes the discrepancy in FPAR between coarse and fine resolution retrievals. In general, both RDL and RDFPAR increase with decreasing resolution because of the nonlinear relation between reflectances and LAI/FPAR (Fig. 6; RDFPAR results are not shown for brevity), as noted previously by Weiss et al. (2000). The contour plots further highlight the importance of cover heterogeneity (Fig. 6), that is, the degree of pixel heterogeneity (dominant land cover purity) determines the discrepancy between coarse and fine resolution retrievals, and thus, the dependence of the algorithm on the spatial resolution of the data.

We note that RDL values in the case of Needle Forests are in general higher compared to other biomes. This is possibly due to the unique reflectance features of needle leaf canopies. Here, the role of canopy architecture is paramount, and when these canopies are mixed with other biome types, the pixel reflectances are significantly altered, thus, resulting in larger RDL values. As an example, we compare the NDVI vs. LAI relation for Needle Forests to that of Shrubs and Grasses in Fig. 7. These relations show NDVI values computed from red and near-infrared reflectances input to the algorithm and the corresponding LAI retrievals. From these relations, we can argue how differently the input reflectance data were translated to LAI by the algorithm in these biomes. From Table 1, we note that among the biomes, Grasses are most commonly mixed with Needle Forests. Hence, large RDL values in the case of Needle Leaf Forests.

The LAI/FPAR retrieval algorithm utilizes the Look-Up-Table (LUT) of the dominant biome of a pixel in the course of retrieval. The presence of other biomes in the case of heterogeneous pixels leads to error in LAI and FPAR retrievals. Thus, it is of interest to evaluate the impact of minority biome presence on LAI retrievals of heterogeneous

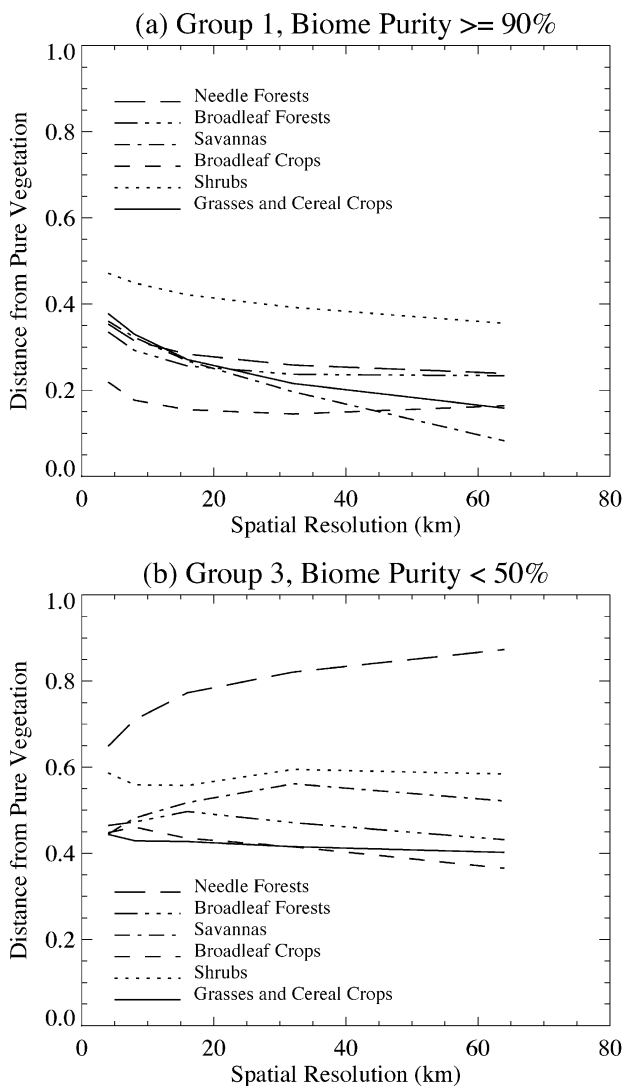


Fig. 5. Average distance in spectral space between biome specific spectral signature  $(\bar{R}, \bar{N})$  and pixels from (a) group 1, and (b) group 3, at different spatial resolutions. Groups 1 and 3 represent biome purities  $\geq 90\%$  and  $< 50\%$ , respectively. The parameters  $\bar{R}$  and  $\bar{N}$  are mean red (RED) and near-infrared (NIR) reflectance values of homogeneous pixels from group 1. See text for further information.

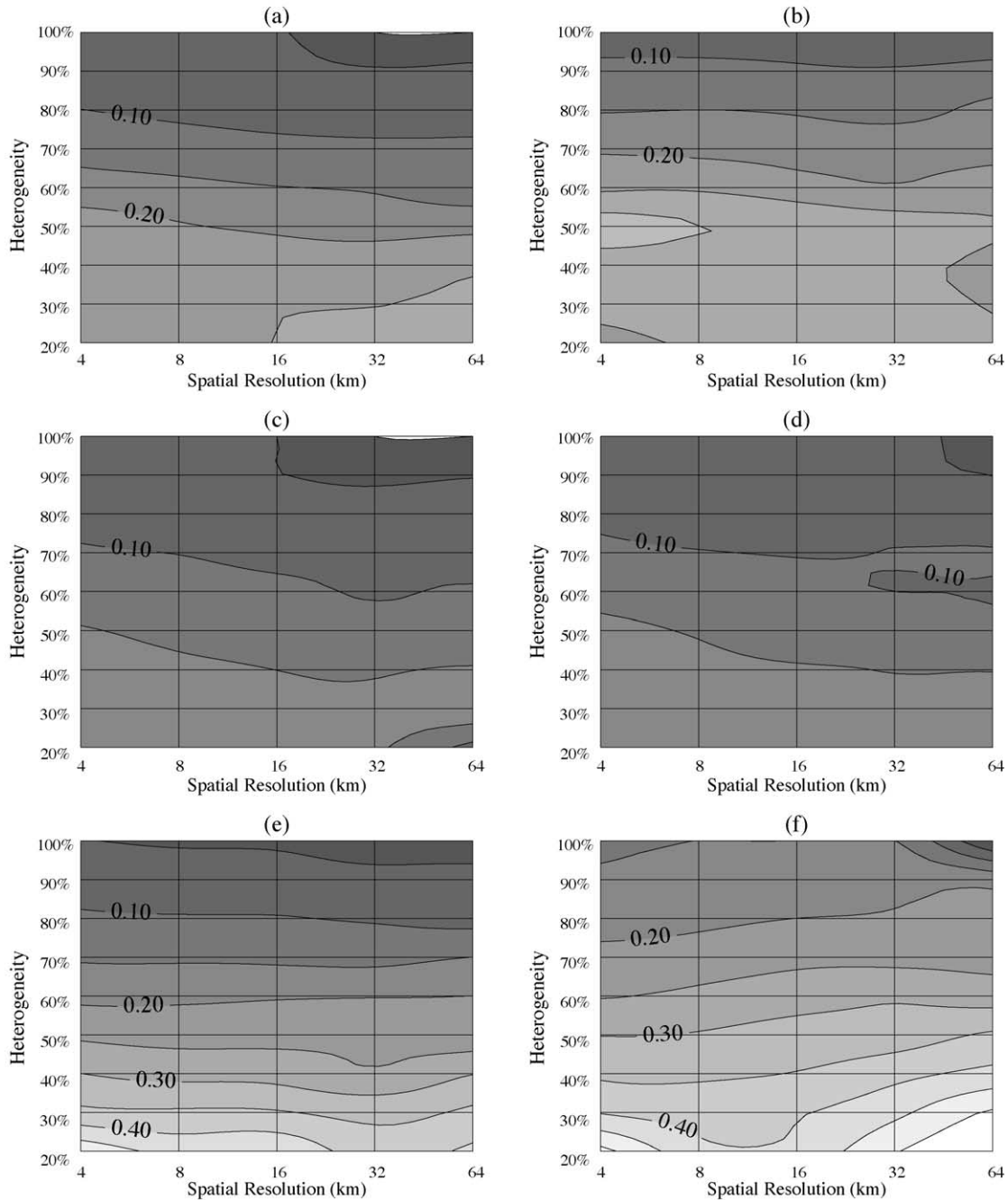


Fig. 6. Contour plot of relative difference in LAI derived from unadjusted LAI retrieval algorithm as a function of spatial resolution and pixel heterogeneity (dominant land cover purity): (a) Grasses and Cereal Crops, (b) Shrubs, (c) Broadleaf Crops, (d) Savannas, (e) Broadleaf Forests, and (f) Needle Forests.

pixels. This is illustrated in Fig. 8, where for each of the biomes, the relative differences in LAI are shown as a function of increasing fractions of minority biome type at a 8-km resolution. It appears that larger LAI errors are incurred when forests are minority biomes in non-forest pixels compared to when forest biomes are mixed with one another. Likewise, larger LAI errors are incurred when non-forest biomes are a minority biome in forest pixels compared to when non-forest biomes are mixed with one another. This is in a way not surprising considering the

difference in architecture, that is, the presence of woody biomass, clumping and structural heterogeneity, between forest and non-forest biomes.

#### 4. Physically based theory for scaling

Most of the algorithms that estimate surface biophysical parameters from remote sensing data use vegetation maps as a priori information to constrain the parameter space. A

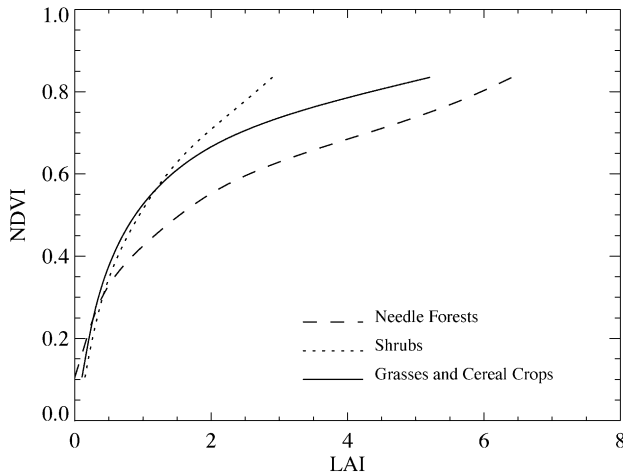


Fig. 7. NDVI-LAI relations derived from the 4-km resolution pixels with purity  $\geq 90\%$ .

common problem with land cover characterization is one of mixture. The designated biome type may be just the dominant biome type, and other biomes can exist within the coarse resolution pixel. Pixel heterogeneity is an important factor causing variations in surface reflectance data (Fig. 3). This information should therefore be taken into account in algorithms in order to correctly interpret data of different resolutions. In this section, we consider a related but wider problem, i.e., fusion of biophysical parameters derived from data acquired by spectroradiometers of different spectral bands and different resolutions.

#### 4.1. Definition and background information

Consider two hypothetical spectroradiometers of resolutions, say, 8 and 1 km and which measure at different wavelength bands. Let  $R(\lambda)$  be the surface reflectances of a 8- by 8-km vegetated pixel at wavelength  $\lambda = \lambda_1, \lambda_2, \dots, \lambda_n$  provided by the first instrument (instrument 1). Let the same pixel be sensed by the second instrument (instrument 2) and  $r_i(\beta)$ ,  $i = 1, 2, \dots, 64$  be surface reflectances at wavelength  $\beta = \beta_1, \beta_2, \dots, \beta_m$  at 1-km resolution covering the 8- by 8-km pixel. Suppose that one uses instruments 1 and 2 reflectance data independently to produce biophysical parameters at 8- and 1-km resolution. The fusion (or scaling, if only the spatial dimension is considered) is said to be accomplished if the biophysical variable at 8-km resolution is equal to the mean value of the 1-km resolution retrievals.

Our theoretical investigation is based on the assumption that the transport equation can describe the radiative regime in vegetation canopies. This equation has a very simple physical interpretation; it is a mathematical statement of the energy conservation law. However, it has been mentioned by many investigators that the transport equation in its original form (Ross, 1981) cannot describe certain aspects of the radiation regime in vegetation canopies because it does not account for the hot spot effect, i.e., a very sharp

delta-function like maximum about the retro-solar direction (Marshak, 1989; Verstraete, Pinty, & Dickenson, 1990; Kuusk, 1985; Myneni et al., 1991; Nilson, 1991; Knyazikhin, Marshak, & Myneni, 1992; Li & Strahler, 1992). Attempts were made to modify it for fitting the observable reflection (Marshak, 1989; Verstraete et al., 1990; Kuusk, 1985; Myneni et al., 1991; Nilson, 1991; Knyazikhin et al., 1992; Li & Strahler, 1992). As a result, a rather wide family of canopy radiation models designed to account for the hot spot effect conflict with the law of energy conservation (Knyazikhin, Martonchik, Diner, et al., 1998). Recently, Zhang, Shabanov, Knyazikhin, & Myneni (2002) showed that the solution of the transport equation contains a singular component which has been ignored in all studies on three-dimensional radiative transfer problems. The singular component is responsible for the hot spot effect. This result justifies the use of the transport equation as the basis for interpretation of remotely sensed data acquired over vegetated land surface.

Let the domain in which the vegetation canopy is located be a parallelepiped  $P$ . Assume that its horizontal and vertical dimensions coincide with the area of the pixel and the tallest tree, respectively. We term this parallelepiped  $P$  as a 3D pixel, or simply, pixel. The top,  $\delta P_T$ , base,  $\delta P_B$ , and lateral surfaces,  $\delta P_L$ , of the parallelepiped  $P$  form its boundary  $\delta P = \delta P_T + \delta P_B + \delta P_L$ . The radiation regime in this medium is described by the three-dimensional transport equation (Ross, 1981; Myneni, 1991; Zhang et al., 2002)

$$\begin{aligned} \Omega \cdot \nabla I_\lambda(r, \Omega) + \sigma(r, \Omega)I_\lambda(r, \Omega) \\ = \int_{4\pi} \sigma_{S,\lambda}(r, \Omega' \rightarrow \Omega)I_\lambda(r, \Omega') d\Omega' . \end{aligned} \quad (3a)$$

Here  $I_\lambda$  (in  $\text{sr}^{-1}$ ) is the monochromatic radiance normalized by the intensity of monodirectional radiation incident on the top surface of the canopy boundary. It depends on wavelength  $\lambda$ , location  $r$ , and direction  $\Omega$ ;  $\sigma_{S,\lambda}$  is the differential scattering cross-section, and  $\sigma = G(r, \Omega)u_L(r)$  is the total interaction cross-section which does not depend on wavelength (Ross, 1981). The geometry factor  $G(r, \Omega)$  (dimensionless) is the mean projection of leaf normals at  $r$  onto a plane perpendicular to the direction  $\Omega$ . It satisfies the following condition

$$\int_{2\pi^+} G(r, \Omega) d\Omega = \pi.$$

The leaf area density distribution function  $u_L(r)$  (in  $\text{m}^2/\text{m}^3$ ) is the one-sided green leaf area per unit volume. The leaf area index can be expressed via the total interaction cross-section as

$$\text{LAI} = \frac{\int_{2\pi^+} d\Omega \int_V dr \sigma(r, \Omega)}{\pi X_P Y_P} = \frac{\int_V u_L(r) dr}{X_P Y_P},$$

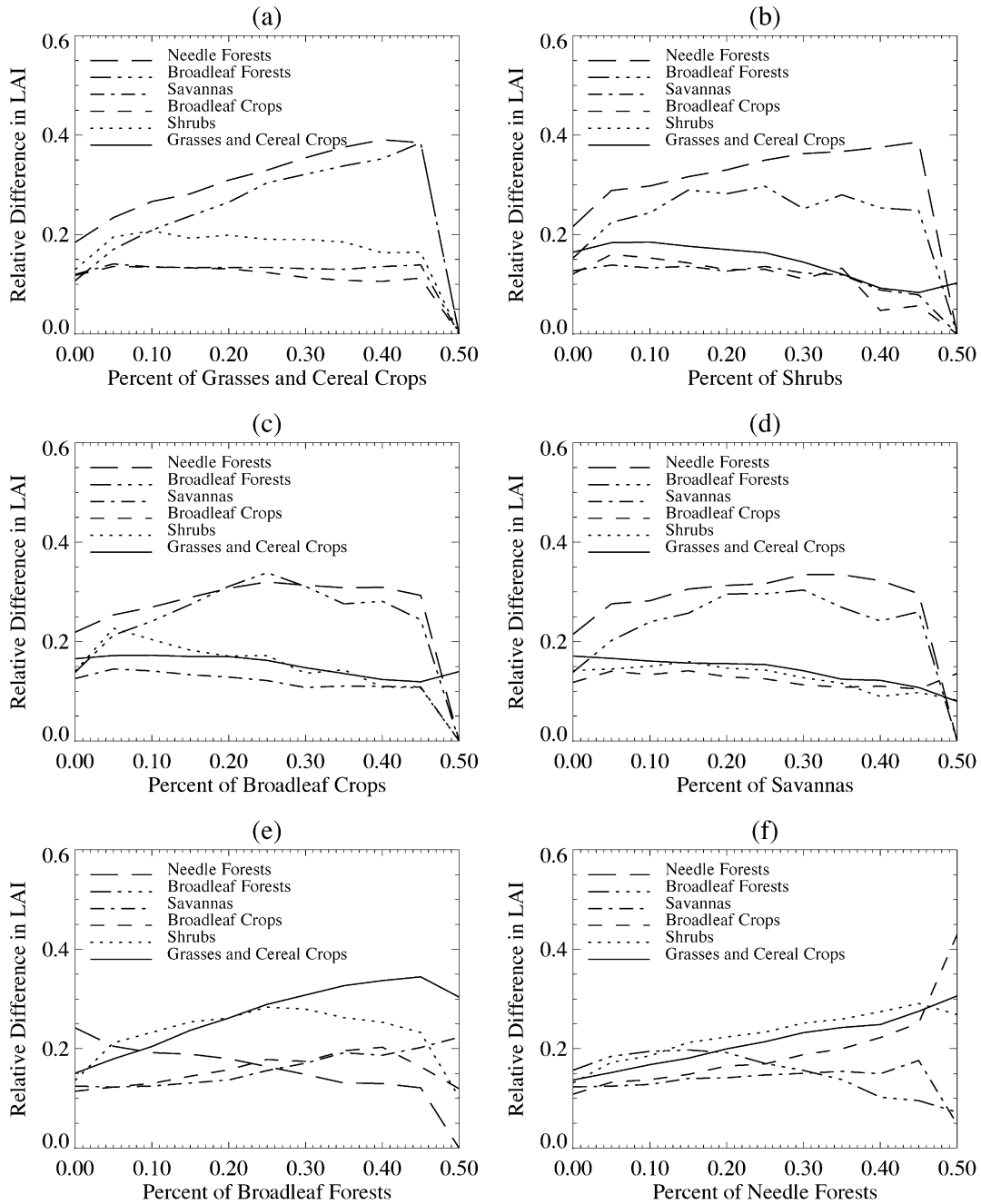


Fig. 8. Relative difference in LAI retrievals as a function of the presence of the minority biome: (a) Grasses and Cereal Crops, (b) Shrubs, (c) Broadleaf Crops, (d) Savannas, (e) Broadleaf Forests, and (f) Needle Forests, in heterogeneous pixels at a 8-km resolution. See text for further information.

where  $X_p$  and  $Y_p$  are horizontal dimensions of the domain  $P$ . A precise description of these variables can be found in Ross (1981) and Myneni (1991). Below, the formulation of Myneni (1991) is adopted.

Let a parallel beam of unit intensity be incident on the upper boundary,  $\delta V_T$ . At the canopy bottom,  $\delta P_B$ , and lateral surfaces,  $\delta P_L$ , the fraction of radiation that is reflected back into the canopy is given by the bi-directional distribution function  $\gamma_\lambda(r_V, \Omega', \Omega)$  of the ground and

lateral surfaces. This case is given by the following boundary conditions:

$$I_\lambda(r_T, \Omega) = \delta(\Omega - \Omega_0), \quad r_T \in \delta P_T, \Omega \cdot n_T < 0, \quad (3b)$$

$$I_\lambda(r_V, \Omega) = \pi^{-1} \int_{\Omega \cdot n_V > 0} \gamma_\lambda(r_V, \Omega', \Omega) I_\lambda(r_V, \Omega') | \Omega' \cdot n_V | d\Omega', \Omega \cdot n_V < 0, r_V \in \delta P_B + \delta P_L. \quad (3c)$$

Here  $n_T$  and  $n_V$  are the outwards normals at points  $r_T \in \delta P_T$  and  $r_V \in \delta P_B + \delta P_L$ , and  $\Omega_0$  is the direction of the parallel beam. Because Eq. (3a) is normalized by the intensity of radiation incident in the direction  $\Omega_0$ , the boundary condition (3b) does not depend on  $\lambda$ .

Solution  $I_\lambda$  of the boundary value problem (Eqs. (3a) and (3b)) can be represented as a sum of two components; that is,

$$I_\lambda(r, \Omega) = I_{bs,\lambda}(r, \Omega) + I_{rest,\lambda}(r, \Omega). \quad (4)$$

The first component,  $I_{bs,\lambda}$ , describes the radiative regime within the vegetation canopy bounded by vacuum on lateral and bottom sides (i.e.,  $\gamma_\lambda = 0$ ; “standard problem”), and  $I_{rest,\lambda}$  describes additional radiative field due to the interaction between the boundary  $\delta P_B + \delta P_L$  and the vegetation canopy. It is well known (e.g., Chandrasekhar, 1960, p. 273; Stamnes, 1982; Box, Gerstl, & Simmer, 1988) that in the case of simple slab geometry and a Lambertian surface (i.e.,  $\gamma_\lambda(r_B, \Omega', \Omega) = \rho_{sur,\lambda}$ ,  $r_B \in \delta P_B$ ) the additional term can be expressed as

$$I_{rest,\lambda} = \rho_{sur,\lambda} F_{bs,\lambda} I_{S,\lambda} / (1 - \rho_{sur,\lambda} r_{S,\lambda}). \quad (5)$$

Here  $F_{bs,\lambda}$  is the downwelling flux at the canopy bottom for the standard problem;  $I_{S,\lambda}$  is the solution to the transport equation with a normalized isotropic source  $q_S = 1/\pi$  (in  $\text{sr}^{-1}$ ) located at the medium bottom (“S” problem), and  $r_{S,\lambda}$  (dimensionless) is the downwelling flux at the medium bottom generated by  $q_S$ . Thus one needs three independent variables to describe the radiative regime in the plane-parallel medium. They are (i) reflectance properties of the underlying surface, which do not depend on the medium; (ii)  $I_{bs,\lambda}$  and (iii)  $I_{S,\lambda}$ , which are surface-independent parameters since no multiple interaction of radiation between the medium and underlying surface is possible, i.e., these variables have intrinsic canopy information.

Somewhat more complicated techniques, adjoint formulation and Green’s function concept, have been developed to extend the representations (4) and (5) for the case of three-dimensional radiation fields (Bell & Glasstone, 1970; Germogenova, 1986; Ioltukhovski, 1999; Knyazikhin, Martonchik, Myneni, et al., 1998; Knyazikhin & Marshak, 2000). Our investigation is based on an approximation of the boundary value problem (Eqs. (3a)–(3c)) by Eqs. (4) and (5) proposed in Knyazikhin et al. (1998) (see also Appendix A). Uncertainties in such an approximation are assumed to be known which are input to MODIS and MISR LAI/FPAR algorithms (Knyazikhin, Martonchik, Diner, et al., 1998; Knyazikhin, Martonchik, Myneni, et al., 1998). In this case, the energy conservation law can be written as

$$r_\lambda = r_{bs,\lambda} + \frac{\rho_{sur,\lambda}}{1 - \rho_{sur,\lambda} r_{S,\lambda}} t_{bs,\lambda} t_{S,\lambda},$$

$$r_{bs,\lambda} + t_{bs,\lambda} + a_{bs,\lambda}$$

$$= 1, \quad r_{S,\lambda} + t_{S,\lambda} + a_{S,\lambda} = 1. \quad (6)$$

Here  $r_{bs,\lambda}$ ,  $t_{bs,\lambda}$ , and  $a_{bs,\lambda}$  ( $r_{S,\lambda}$ ,  $t_{S,\lambda}$ , and  $a_{S,\lambda}$ ) are canopy reflectance, transmittance and absorptance for the standard problem (for the “S” problem).

It was shown (Knyazikhin, Martonchik, Diner, et al., 1998; Knyazikhin, Martonchik, Myneni, et al., 1998; Panferov et al., 2001) that, in the case of the standard and S problems, some simple algebraic combinations of leaf and canopy spectral transmittances and absorptances eliminate their dependencies on wavelength through the specification of two canopy-specific wavelength independent variables. Under the above assumptions, these variables and leaf optical properties govern the law of energy conservation (6) in vegetation canopies at any given wavelength of the solar spectrum. These results constitute the basis for our approach to scaling, or more broadly, fusion, in the sense of the definition given previously.

#### 4.2. Spatial resolution-dependent radiative transfer formulation

Solar radiation scattered from a vegetation canopy and measured by satellite-borne sensors results from interaction of photons traversing through the foliage medium, bounded at the bottom by a radiatively participating surface. Therefore, to estimate the canopy reflectance, three important variables must be carefully formulated: the architecture of the canopy, the optical properties of foliage elements, and the background surface reflectance properties. Specification of the first two variables depends on the definition of the foliage element or scattering center. An individual leaf, for example, should be taken as the basic foliage element to describe photon transport in a vegetation canopy of a small area (about 0.1–0.3 ha) (Knyazikhin, Miessen, Panferov, & Gravenhorst, 1997). Optical properties of tree crowns and their distribution in the canopy space can be used to estimate the radiation regime in an extended canopy. In both cases, the three-dimensional transport equation relates properties of the scattering centers to the radiative regime of the medium. The former allows estimation of the radiation field at the leaf scale, while the latter describes the interaction of photons with trees, which is appropriate for interpretation of reflectances at coarse resolution. The reflective properties of the tree crown are determined by its leaf optical properties and architecture. Therefore, solutions of the transport equation that describe canopy radiation regime at the leaf and crown scales are not independent. This allows us to relate these solutions to the biophysical parameters defined at different scales, or spatial resolutions. The major issue is, of course, how the coefficients appearing in the transport equation vary with spatial resolution.

Consider the vegetation canopy located in the pixel  $P$ . To approximate the canopy structure, we introduce a spatial mesh by dividing  $P$  into fine grid cells. We term the ratio  $R$ , the total number of cells in  $P$  to the volume of  $P$ , as the resolution of the model, or a scale at which photon transport and interaction are formulated. This parameter determines

the accuracy in the modeled mean radiation quantities of the pixel (Knyazikhin et al., 1997).

Photons interact with scattering centers that reside in these cells. We assume that, for a cell containing  $M$  scattering centers, the intensity scattered by the cell is the sum of intensities scattered by the individual scattering centers (Van de Hulst, 1981). That is, photons experience only a single interaction with the scattering centers inside the cell. This assumption allows the use of the radiative transfer equation to describe photon interactions with scattering centers. Thus, the total interaction and differential scattering cross-sections that appear in the transport equation are cell averages of the cross-sections calculated for individual scattering centers. The solution of the transport equation provides mean intensity over the cell around the spatial point  $r$  in direction  $\Omega$  (Ross, 1981, p. 144).

The specification of the scattering centers and scale  $R$  must be consistent in order to predict correct canopy reflectance for the pixel. For example, in the case of a coniferous forest (*Picea abies* (L.) Karst) of domain  $P=25 \times 30 \times 29$  m, a model resolution of  $R=8$  (or cell size of  $50 \times 50 \times 50$  cm) and a 1-year shoot of size 5–7 cm as the scattering center guarantees accurate evaluation of mean canopy reflectance over a horizontal area of about  $10 \text{ m}^2$  (Knyazikhin et al., 1997). It should be emphasized that the scattering properties of the shoot must be known in order to formulate the differential scattering cross-section. At this scale, a single needle cannot be taken as the scattering center because photons undergo multiple interactions within the shoot, and thus, the above assumption is violated for a cell of  $50 \times 50 \times 50$  cm.

In this manner, we introduce three spatial attributes of the medium, namely, pixel size, scale, and scattering centers to describe its radiative behavior. Under the consistency assumption, the radiation regime in this medium can be described by the three-dimensional transport Eq. (3a). The total interaction cross-sections,  $\sigma$ , and the differential scattering cross-sections,  $\sigma_{S,\lambda}$ , depend on the scale  $R$  and the definition of the scattering centers. The reflectance measured by satellite-borne sensors is the solution to the boundary value problem (Eqs. (3a)–(3c)) averaged over the pixel. By definition, the total interaction cross-section  $\sigma ds$  is the probability that a photon, while traveling a distance  $ds$ , hits a scattering center. Because the photon interacts with leaves at any wavelength, this probability is wavelength independent.

The magnitude of scattering per volume unit is described using the single scattering albedo

$$\omega_\lambda(R, r, \Omega) = \frac{\int_{4\pi} \sigma_{S,\lambda}(R, r, \Omega \rightarrow \Omega') d\Omega'}{\sigma(R, r, \Omega)}.$$

Let  $g_\lambda(R, r, \Omega \rightarrow \Omega')$  be the differential scattering cross-section normalized by the single scattering albedo, i.e.,

$\sigma_{S,\lambda}(R, r, \Omega \rightarrow \Omega') = \omega_\lambda(R, r, \Omega)g_\lambda(R, r, \Omega \rightarrow \Omega')$ . For simplicity, the single scattering albedo is assumed constant with respect to spatial,  $r$ , and directional,  $\Omega$ , variables, and  $g$  is independent of wavelength. In this case, the solutions  $I_{bs,\lambda}$  and  $I_{S,\lambda}$  depend on values of the spectral single scattering albedo, which in turn depends on wavelength. This allows their parameterization in terms of single scattering albedo rather than wavelength. Therefore, wavelength dependence will be suppressed in further notations. The value of the single scattering albedo  $\omega$  will be added to the argument list of the solution  $I_{bs,\lambda}$  and  $I_{S,\lambda}$ .

Consider an extended vegetation canopy contained in a parallelepiped  $P$ . Let  $V \subset P$  be another parallelepiped contained in  $P$ . The top,  $\delta V_T$ , base,  $\delta V_B$ , and lateral surfaces,  $\delta V_L$ , of the parallelepiped  $V$  form its boundary  $\delta V = \delta V_T + \delta V_B + \delta V_L$ . Integration of Eq. (3a) over  $V$  and the full solid angle  $4\pi$  leads to the form of law of energy conservation law (Titov, 1998)

$$A(\omega) + F_T^+(\omega) + F_B^+(\omega) = F_T^-(\omega) + F_B^-(\omega) + F_L^-(\omega) - F_L^+(\omega), \quad (7)$$

where  $A$  is radiant energy absorbed by  $V$ ;  $F_T^\pm$ ,  $F_B^\pm$  and  $F_L^\pm$  are radiant fluxes penetrating into (sign “−”) and exiting (sign “+”) the canopy through the top (subscript “T”), base (subscript “B”) and lateral sides (subscript “L”) of the parallelepiped  $V$ , i.e.,

$$F_\chi^\pm(\omega) = \int_{\delta V_\chi} dS \int_{\pm \Omega \cdot n(r) > 0} I_\omega(R, r, \Omega) |\Omega \cdot n(r)|, \\ \chi = T, B, \text{ or } L.$$

Here,  $n(r)$  is the outward normal at points  $r \in \delta V$ , and  $I_\omega(R, r, \Omega)$  is the solution of boundary value problem (Eqs. (3a)–(3c)). Under assumptions formulated in the previous section, we can restrict our discussion here to the case of a completely absorbing background beneath the canopy, i.e.,  $F_B^- = 0$ .

Titov (1998) introduced horizontal transport of radiant energy as  $E = F_L^- - F_L^+$ . It follows from Eq. (7) that the amount of energy absorbed ( $A/F_L^-$ ), reflected ( $F_L^+/F_L^-$ ), and transmitted ( $F_B^+/F_T^-$ ) by the volume  $V$  is not necessarily equal to 1; it can be greater or less than 1, depending on the sign of  $E$ . The magnitude of horizontal transport depends on mean length,  $l$ , of photon lateral migration in the medium (Titov, 1998). If the horizontal sizes,  $x_V$  and  $y_V$ , of  $V$  are substantially greater than  $l$ , the horizontal transport  $E/F_T^- \ll 1$ . This condition is fulfilled for a horizontally homogeneous medium. If  $x_V, y_V \sim l$ , the average of Eq. (7) over number  $N_x N_y$  of pixels, such that  $N_x x_V \gg l$ ,  $N_y y_V \gg l$ , results in  $E/F_T^- \approx 0$  (Titov, 1998). This property is used to adjust the radiative transfer Eq. (3a) to simulate surface reflectances at a given resolution by choosing an appropriate model resolution  $R$  and definition of the scattering center (Knyazikhin et al., 1997). It means that the definition of scattering centers and model resolution

should be chosen such that the horizontal size of the fine cell is comparable to  $l$ . This allows us to account for horizontal transport within the pixel. The transport equation at this scale can be extended to evaluate surface reflectances of horizontally homogeneous coarse pixels. The reflectance of a heterogeneous coarse pixel, however, cannot be taken as the average of reflectances calculated for fine resolution pixels because this technique does not account for the radiative properties of neighboring pixels. Neglecting horizontal transport can lead to uncontrollable errors in the interpretation of measured data (Titov, 1998). The transport equation, therefore, should be adjusted for the resolution of data.

#### 4.3. Scaling of reflection and absorption properties of scattering centers

Consider a volume  $V$  that can be taken as the scattering center. The radiative response of  $V$  at a point  $r \in V$  to a point mono-directional source located at a point  $r_0$  on the boundary  $\delta V$  of the volume  $V$  is the Green's function,  $G(r_0, r, \Omega_0 \rightarrow \Omega)$ , where  $\Omega_0$  and  $\Omega$  are directions of the incident and reflected radiation streams, respectively (Case & Zweifel, 1967). The volume Green's function satisfies Eq. (3a) and the boundary condition

$$G(r_0, r_V, \Omega_0 \rightarrow \Omega) = \delta(r_V - r_0) \delta(\Omega - \Omega_0), \quad (8)$$

$$r_V \in \delta V.$$

The extinction coefficient  $\sigma$ , the single scattering albedo  $\omega$ , and the normalized differential scattering cross-section  $g$  which characterize properties of the volume  $V$  at the fine scale  $R_0$  are assumed known. We investigate properties of Green's function using operator theory (Vladimirov, 1963; Richtmyer, 1978) by introducing the differential,  $L$ , and integral,  $S$ , operators,

$$LI = \Omega \cdot \nabla I + \sigma(R_0, r, \Omega) I(r, \Omega);$$

$$SI = \int_{4\pi} g(R_0, r, \Omega' \rightarrow \Omega) I(r, \Omega') d\Omega'.$$

Given the assumption above regarding the single scattering albedo  $\omega$  and the normalized differential scattering cross-section  $g$ , the differential and integral operators are wavelength independent. In terms of these notations, the equation for the Green's function can be rewritten as  $LG = \omega SG$ . Its solution  $G_\omega$  can be represented as the sum, i.e.,  $G_\omega = Q + \varphi_\omega$ . Here, the wavelength independent function  $Q$  is the probability density that a photon in the direct beam will arrive at  $r$  along the direction of incident radiation without suffering a collision. It satisfies the equation  $LQ = 0$  and the boundary conditions specified by Eq. (8). The second term,  $\varphi_\omega$ , describes photons scattered in the volume  $V$ . It satisfies  $L\varphi_\omega = \omega S\varphi_\omega + \omega SQ$  and zero boundary con-

ditions. By stating  $T = L^{-1}S$ , the transfer equation for  $\varphi_\omega$  can be transformed to

$$\varphi_\omega = \omega T\varphi_\omega + \omega TQ.$$

Substituting  $\varphi_\omega = G_\omega - Q$  into this equation results in an operator equation for  $G_\omega$  (Zhang et al., 2002)

$$G_\omega - \omega TG_\omega = Q. \quad (9)$$

It follows from Eq. (9) that  $G_\omega - \omega TG_\omega$  does not depend on  $\omega$ , and involves the validity of the following relationship

$$G_\omega - \omega TG_\omega = G_\alpha - \alpha TG_\alpha = Q, \quad (10)$$

where  $G_\omega$  and  $G_\alpha$  are Green's functions corresponding to single scattering albedos  $\omega$  and  $\alpha$ , respectively. Eq. (10) was originally derived by Zhang et al. (2002).

Let  $i(V, \omega)$  be volume absorption  $a(V, \omega)$  normalized by  $1 - \omega$ , i.e.,  $i(V, \omega) = a(V, \omega)/(1 - \omega)$ . This variable is the average number of photon interactions with the scattering centers in  $V$  before either being absorbed or exiting  $V$ . It can be expressed via Green's function as

$$i(V, \omega) = \frac{\int_{4\pi} d\Omega' \int_V dr \sigma(R_0, r, \Omega) G_\omega(r_0, r, \Omega_0 \rightarrow \Omega') / |n(r_0) \cdot \Omega_0|}{|n(r_0) \cdot \Omega_0|}. \quad (11)$$

Multiplying Eq. (10) by the extinction coefficient  $\sigma$  and integrating over  $V$  and all directions  $\Omega$  result in

$$i(V, \omega) - \omega p_i(\omega) i(V, \omega) = i(V, \alpha) - \alpha p_i(\alpha) i(V, \alpha) = q(V). \quad (12)$$

Here

$$p_i(\omega) = \frac{\int_V dr \int_{4\pi} \sigma(R_0, r, \Omega) \psi_\omega(R_0, r, \Omega) d\Omega}{i(\omega) |n(r_0) \cdot \Omega_0|}, \quad (13a)$$

$$q(V) = \frac{\int_{4\pi} d\Omega \int_V dr \sigma(R_0, r, \Omega) Q(r, \Omega)}{|n(r_0) \cdot \Omega_0|}, \quad (13b)$$

where  $\psi_\omega = TG_\omega$ . The coefficient  $p_i(\omega)$  is approximated by  $p_0(V)$ , where  $p_0(V)$  is the positive eigenvalue of the operator  $T$  (Appendix A) which is determined by intrinsic structural properties of  $V$ . Eq. (12) expresses the energy conservation law for the volume  $V$ .

The coefficient  $q(V)$  is the probability that a photon entering  $V$  along  $\Omega_0$  will undergo one interaction with scattering centers defined at the scale  $R_0$ . Given  $q(V)$ , one can derive the extinction coefficient for another volume consisting of scattering centers  $V$ . The absorption and reflection properties of this coarse volume are determined by  $a(V, \omega) = q(V)[1 - \omega]/[1 - p_0(V)\omega]$  and Green's function  $G_\omega$ . These coefficients describe photon interactions with

vegetation at coarse scale  $R$  that, in turn, are determined by photon transport at the fine scale  $R_0$ .

#### 4.4. Scaling of surface reflectances

Consider an extended vegetation canopy that occupies a parallelepiped  $P$  of horizontal dimensions  $X_P$  and  $Y_P$ . Under assumptions formulated earlier, we can restrict our discussion here to the standard problem. The pixel  $P$  consists of  $N$  fine resolution pixels  $P_k$ ; that is,  $P = \sum_{k=1}^N P_k$ . Let  $R_0$  be the scale of  $P_k$ . Attenuation and scattering of photons within the fine resolution pixel  $P_k$  is given by the total interaction cross-section  $\sigma_k$  and the single scattering albedo  $\omega_k$ . These variables are assumed to be constant with respect to the spatial variable  $r$  within  $P_k$  and take on a zero value outside the pixel  $P_k$ . This allows us to express the total interaction cross-section  $\sigma$  and the single scattering albedo  $\omega$  for the coarse pixel  $P$  at the scale  $R_0$  as

$$\sigma(R_0, r, \Omega) = \sum_{k=1}^N \sigma_k(R_0, \Omega), \quad \omega(R_0, r) = \sum_{k=1}^N \omega_k(R_0).$$

Note that the single scattering albedo for the pixel  $P$  depends on the spatial variable  $r$ . Let a parallel beam of unit intensity be incident on the upper boundary of  $P$  along  $\Omega_0$ . Multiplying Eq. (3a) by the extinction coefficient  $\sigma$  and integrating over  $P$  and all directions  $\Omega$  and normalizing by  $X_P Y_P \mu_0$ , where  $\mu_0 = |n_0 \cdot \Omega_0|$ , and  $n_0$  is the outward normal to the upper boundary of  $P$ , one obtains

$$i(P) - \sum_{k=1}^N \omega_k \langle \sigma_k \Psi \rangle_{P_k} = q(P). \quad (14)$$

Here  $\Psi = TI$ , and  $\langle \cdot \rangle_{P_k}$  denotes integration over  $P_k$  and the full solid angle  $4\pi$  normalized by  $X_P Y_P \mu_0$ .

Let  $p_0(P)$  be the positive eigenvalue of the operator  $T$  corresponding to the scale  $R_0$  (Knyazikhin, Martonchik, Diner, et al., 1998; Knyazikhin, Martonchik, Myneni, et al., 1998). Integrating Eq. (11) over the upper boundary of  $P$  and accounting for Eq. (12) result in  $p_0(P) \approx \langle \sigma \Psi \rangle_P / i(P)$ . This involves

$$\langle \sigma_k \Psi \rangle_{P_k} = \frac{\langle \sigma_k \Psi \rangle_{P_k}}{i(P)} i(P) = \frac{\langle \sigma_k \Psi \rangle_{P_k}}{\langle \sigma \Psi \rangle_P} i(P) p_0(P).$$

The latter allows us to approximate Eq. (14) as

$$i(P) - \omega p_0(P) i(P) = q(P), \quad (15)$$

where

$$\omega = \sum_{k=1}^N \omega_k \frac{\langle \sigma_k \Psi \rangle_{P_k}}{\langle \sigma \Psi \rangle_P}, \quad (16)$$

is the single scattering albedo at a scale that accounts for photon interaction with sub-pixels  $P_k$ . The solution of the

transport equation corresponding to the single scattering albedo  $\omega$  satisfies the energy conservation relationship specified by Eq. (15). This shows that a re-evaluation of the single scattering albedo is required to force the transport equation formulated at scale  $R_0$  to simulate coarse pixel reflectances without violating the energy conservation law. It also means that the single scattering albedo is the basic parameter of the transport equation that describes variations in surface reflectance due to changing spatial resolution.

#### 4.5. Scaling of LAI field

We adjusted the transport equation as described above to simulate the radiation regime in vegetation canopies bounded by a parallelepiped  $P_0$  of horizontal dimensions  $30 \times 30$  m with an uncertainty of 20% (Knyazikhin et al., 1997). The model resolution is  $R_0 = 8$ . A single leaf and a 1-year shoot of size 5–7 cm were taken as scattering centers in Broadleaf and Needle Forests, respectively. The single scattering albedo coincides with leaf albedo in this case, which is defined as the fraction of incident radiation flux density that the leaf transmits and reflects. The leaf albedo is a measurable parameter. A data bank of leaf optical properties was assembled from various sources, and analyzed to obtain the mean and variance spectrum as a function of biome type. This information is used to model canopy reflectance at a 30-m resolution.

For the purpose of LAI and FPAR retrieval, global vegetation is stratified into six architectural types or biomes (Myneni et al., 1997) as mentioned previously. Each biome is represented by wavelength independent eigenvalues of the operator  $T$  that quantify canopy structures, wavelength-dependent patterns of ground reflectances and one single pattern of leaf spectral albedo per biome. The solution of the transport equation can be expressed explicitly in terms of these variables (Knyazikhin, Martonchik, Diner, et al., 1998; Knyazikhin, Martonchik, Myneni, et al., 1998). Thus, surface reflectances can be simulated as a function of resolution and wavelength bands of the spectroradiometer.

It follows from the parameterization of global vegetation, that Eq. (16) contains six different values of the single scattering albedo. Therefore,

$$\omega = \sum_{l=1}^6 \omega_l \sum_{\omega_k = \omega_l} \frac{\langle \sigma_k \Psi \rangle_{P_k}}{\langle \sigma \Psi \rangle_P}. \quad (17)$$

A rough estimation of Eq. (17) can be performed as follows. One approximates the solution  $I$  in the definition of  $\Psi$  by the normalized positive everywhere eigenvector  $e_k$  of the operator  $T$  defined on  $P_k$ . This yields

$$\begin{aligned} \langle \sigma_k T e_k \rangle_{P_k} &= \langle \sigma_k P_k(P_k) e_k \rangle_{P_k} \\ &= \frac{p(P_k) \int_{4\pi} d\Omega \int_{P_k} \sigma_k e_k(r, \Omega) dr}{X_P Y_P |\mu_0|} = \frac{p(P_k)}{X_P Y_P |\mu_0|}. \end{aligned}$$

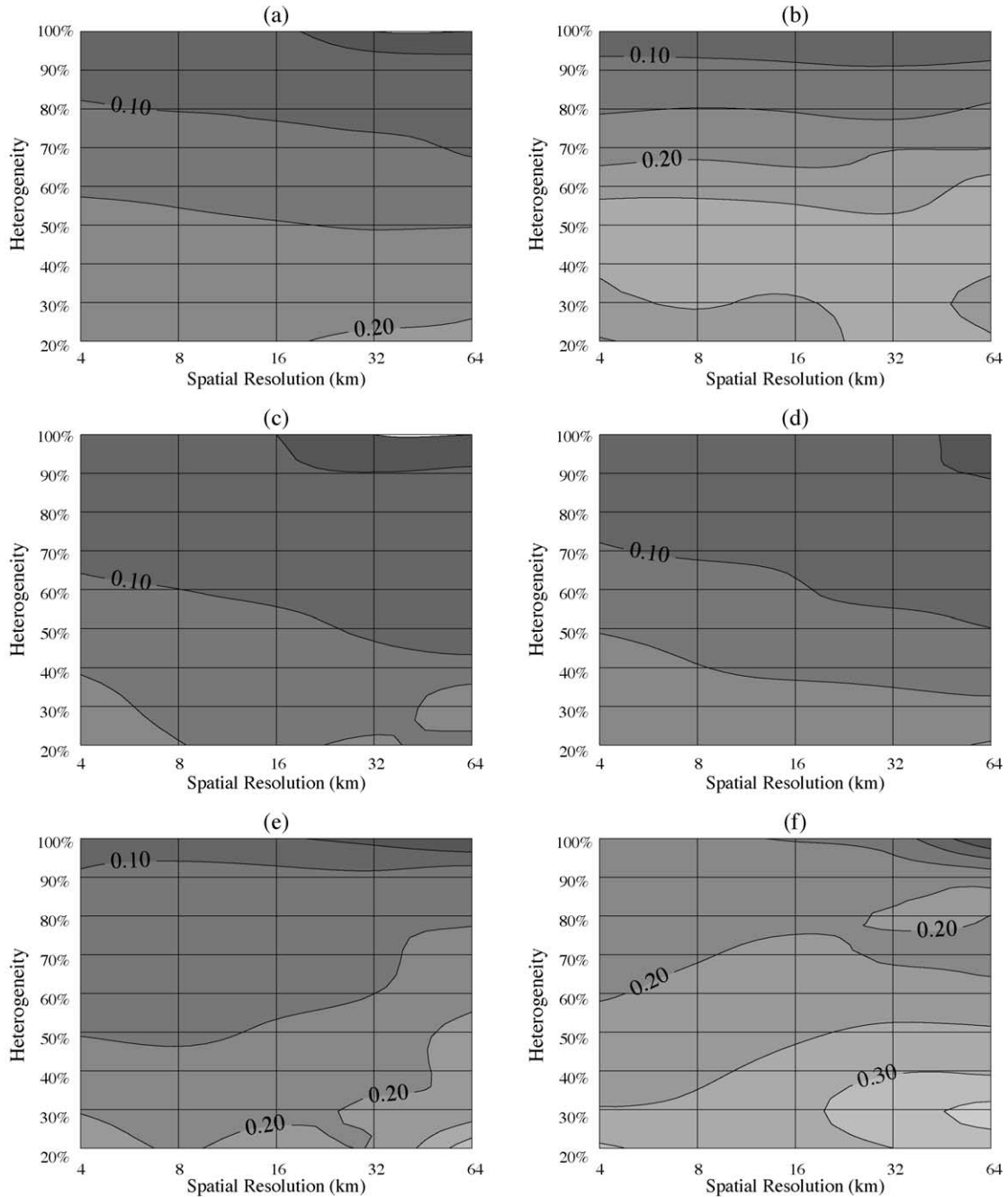


Fig. 9. Contour plot of relative difference in LAI derived from adjusted LAI retrieval algorithm as a function of spatial resolution and pixel heterogeneity (dominant land cover purity): (a) Grasses and Cereal Crops, (b) Shrubs, (c) Broadleaf Crops, (d) Savannas, (e) Broadleaf Forests, and (f) Needle Forests.

The eigenvalue  $p(P_k)$  is determined by the intrinsic structural properties of  $P_k$  and takes on values between 0 and 1 (Knyazikhin and Marshak, 1991). Assuming that the structure of a given biome type has equal probability of occurrence, the average value of  $p(P_k)$  over biome type is 0.5. Let  $N_k$  and  $N_{\text{veg}}$  be the number of pixels  $P_k$  belonging to biome  $k$  and the total number of vegetated pixels  $P_k$ , respectively. Taking into account  $\sigma_k = 0$  for non-vegetated pixel, one obtains

$$\sum_{\omega_k = \omega_l} \frac{\langle \sigma_k \Psi \rangle_{P_k}}{\langle \sigma \Psi \rangle_P} = \frac{N_l}{N_{\text{veg}}} = \frac{\text{pf}_l}{1 - \text{pf}_7}. \quad (18)$$

Substituting Eq. (18) into (17) results in

$$\varpi = \frac{1}{1 - \text{pf}_7} \sum_{l=1}^6 \omega_l \text{pf}_l. \quad (19)$$

Thus, given the percentage function  $\text{pf}_l$  ( $l = 1, \dots, 7$ ) of each coarse resolution pixel, one can redefine the single scattering albedo according to Eq. (19). The use of this single scattering albedo in Eq. (9) results in a relationship for canopy transmittance similar to Eq. (13a) with a wavelength independent constant determined by the operator  $T$ . Solution

of the transport Eq. (3a) with this single scattering albedo, therefore, provides a correct partition of incoming solar radiation between canopy reflection, transmission and absorption.

The realization of this radiative transfer based scaling theory is illustrated in Fig. 9, where the relative discrepancy in retrieved LAI (RDL; Eq. (2)) is shown as a function of spatial resolution and pixel heterogeneity for the six biomes. Note that the RDL does not exceed the uncertainty in the model used simulate radiation regime in vegetation canopies at the scale  $R_0=8$ . This figure is similar to Fig. 6, except that the Look-Up-Tables of the LAI/FPAR estimation algorithm have been tuned based on theoretical considerations given above. We note a dramatic decrease in RDL in all cases, including the case of large pixels with significant heterogeneity. Based on the definition of RDL, which is the difference between  $L_t$  and  $L_c$  (Eq. (2)), tuning of the Look-Up-Tables by adjusting the single scattering albedo as per Eq. (19) to minimize RDL, constitutes the physics based approach to scaling. Also, this is consistent with our definition of scaling, given earlier as, the process by which it is established that values of a certain biophysical product, LAI in this instance, derived from coarse resolution sensor data equal the arithmetic average of values derived independently from fine resolution sensor data. It should be noted uncertainties in the reference 1-km LAI field are unknown, and thus, the RDL does not characterize the quality of retrievals. However, the RDL indicates that the proposed technique can reduce scaling errors due to spatial scale effects.

## 5. Concluding remarks

The effect of spatial resolution of reflectance data on retrievals of LAI is addressed in this article. Problems related to data resolution arise in the context of assembling time series of biophysical variables with data from sensors of different spatial resolution, fusion of data of different instruments and in the validation of moderate resolution sensor products. We define the goal of scaling as the process by which it is established that values of a certain biophysical product, LAI in this instance, derived from coarse resolution sensor data equal the arithmetic average of values derived independently from fine resolution sensor data. Pixel heterogeneity is defined in terms of fractional presence of different land covers, for the purposes of scaling. The effect of pixel heterogeneity on spectral reflectances and LAI retrievals is investigated with the 1-km AVHRR data aggregated to different coarse spatial resolutions. Pixel heterogeneity is shown to increase as the resolution of the data decreases. LAI retrieval errors at coarse resolution are inversely related to the proportion of the dominant land cover in such pixel. Further, large errors in LAI retrievals are shown to occur when forests are minority biomes in non-forest

pixels compared to when forest biomes are mixed with one another, and vice versa. A physically based technique for scaling with explicit spatial resolution-dependent radiative transfer formulation was developed. The mean length of photon lateral migration in the medium, which characterizes the magnitude of horizontal transport, is used to imbue resolution dependence to the radiative transfer equation. Spatial resolution dependence of absorption and reflection properties of the scattering centers is accomplished via the use of a Green's function formulation. Pixel heterogeneity is accounted by modifications to the single scattering albedo that the transfer equation admits through the use of land cover fractions. The successful application of this theory to scaling LAI retrievals from AVHRR data of different resolutions demonstrates a capability to validate moderate resolution ( $\sim 1$  km) LAI and FPAR products from MODIS and MISR. It should be noted that our empirical study only considers scaling error between 1 km and coarser scales and is targeted specifically data sets coarser than 1 km. Therefore, replication of our empirical study with a 30-m fine resolution imagery over large areas is needed.

## Acknowledgements

This research was supported by NASA through MODIS Contract NAS5-96061. Jan Bogaert is a Postdoctoral Fellow of the Fund for Scientific Research-Flanders. We thank R. Fernandes for stimulating discussions.

## Appendix A

Consider Eq. (3a) with boundary conditions expressed by Eqs. (3b) and (3c). In the MODIS and MISR LAI/FPAR retrieval algorithm, the boundary conditions (Eq. (3c)) for the lateral surface and base of the domain  $P$  are replaced by vacuum conditions, i.e.,  $\gamma_\lambda(r_L, \Omega, \Omega') = 0$  ( $r_L \in \delta V_L$ ) and  $\gamma_\lambda(r_B, \Omega, \Omega') = \rho_{\text{sur}, \lambda} \gamma_0(r_B, \Omega)$  ( $r_B \in \delta V_B$ ). Here  $\rho_{\text{sur}, \lambda}$  and a wavelength independent function  $\gamma_0(r_B, \Omega, \Omega')$  are the effective ground reflectance and anisotropy respectively (Knyazikhin, Martonchik, Diner, et al., 1998; Knyazikhin, Martonchik, Myneni, et al., 1998). Given these assumptions, the solution of the boundary value problem (Eqs. (3b) and (3c)) can be expressed in the forms (4) and (5), where  $I_S$  is the solution to the transport equation with a normalized anisotropic heterogeneous wavelength-independent source,  $\gamma_0(r_B, \Omega, \Omega')$  (in  $\text{sr}^{-1}$ ) located at the surface underneath the vegetation canopy, and  $r_{S, \lambda}$  (dimensionless) is the downwelling flux at the canopy bottom generated by  $\gamma_0(r_B, \Omega, \Omega')$ . Note that boundary conditions of the standard and “S” problems are wavelength independent. This results in a relation between canopy interception  $i_\chi(\lambda_0)$  and transmittance  $t_\chi(\lambda_0)$ , for the standard ( $\chi = \text{“bs”}$ ) and “S” ( $\chi = \text{“S”}$ ) problems at an arbitrary chosen reference wavelength  $\lambda_0$ , and interception

$i_{\chi}(\lambda)$  and transmittances  $t_{\chi}(\lambda)$  at all other wavelengths  $\lambda$  in the solar spectrum (Knyazikhin, Martonchik, Myneni, et al., 1998; Panferov et al., 2001),

$$\begin{aligned} i_{\chi}(\lambda) &= \frac{1 - \omega(\lambda_0)p_0(V)}{1 - \omega(\lambda)p_0(V)} i_{\chi}(\lambda_0), \\ t_{\chi}(\lambda) &= \frac{1 - \omega(\lambda_0)p_{t_{\chi}}(V)}{1 - \omega(\lambda)p_{t_{\chi}}(V)} t_{\chi}(\lambda_0). \end{aligned} \quad (A1)$$

where  $p_0(V)$  and  $p_{t_{\chi}}(V)$  are canopy structure-dependent and wavelength-independent variables. The variable  $p_0(V)$  is the maximum positive eigenvalue of the operator  $T$ .

It follows from Eqs. (A1) and (12) that the equality

$$\frac{i(V, \omega)}{i(V, \alpha)} = \frac{1 - \alpha p_0(V)}{1 - \omega p_0(V)} = \frac{1 - \alpha p_i(\alpha)}{1 - \omega p_i(\omega)},$$

holds true for any  $\alpha$  and  $\omega$ . This relationship can be rewritten as

$$\frac{1 - \alpha p_i(\alpha)}{1 - \alpha p_0(V)} = \frac{1 - \omega p_i(\omega)}{1 - \omega p_0(V)}.$$

The former can be fulfilled for any  $\alpha$  and  $\omega$  if and only if (a)  $p_i(\alpha) = 1/\alpha$  or (b)  $1 - \alpha p_i(\alpha) = 1 - \alpha p_0(V)$ . Let us assume that  $p_i(\alpha) = 1/\alpha$ . Substituting  $p_i(\alpha) = 1/\alpha$  into Eq. (12) results in  $q(V) = 0$ . It follows from Eq. (13b) that  $q(V) > 0$  (if  $\sigma \neq 0$ ) and thus, our assumption is not true. Condition (b) is valid if and only if  $p_i(\alpha) = p_0(V)$ . Thus, if Eq. (A1) is valid the right-hand side of Eq. (13a) does not depend on  $\omega$ . Small deviations of Eq. (A1) from exact equality do not result in large variation in the right-hand side of Eq. (13a).

A similar relationship can be derived for canopy transmittance. It should be emphasized that canopy reflectance  $r_{\chi}(\lambda)$  does not possess the spectral invariant property (A1) (Panferov et al., 2001). This variable should be estimated via the energy conservation law, namely,  $r_{\chi}(\lambda) = 1 - t_{\chi}(\lambda) - a_{\chi}(\lambda)$ .

## References

- Bell, G. I., & Glasstone, S. (1970). *Nuclear Reactor Theory* (p. 619). New York: Van Nostrand-Reinhold.
- Box, M. A., Gerstl, S. A. W., & Simmer, C. (1988). Application of the adjoint formulation of the calculation of atmospheric radiative effects. *Beitrage zur Physik der Atmosphere*, 61, 303–311.
- Case, K. M., & Zweifel, P. F. (1967). *Linear Transport Theory* (p. 342). Reading, MA: Addison-Wesley.
- Chandrasekhar, S. (1960). *Radiative Transfer* (p. 393). Oxford: Clarendon, 1950 (reprinted by Dover, New York (NY)).
- Chen, J. M. (1999). Spatial scaling of a remotely sensed surface parameter by contexture. *Remote Sensing of Environment*, 69, 30–42.
- Cihlar, J., Beaubien, J., Latifovic, R., & Simard, G. (1999). Land cover of Canada Version 1.1. In *Special Publication, NBIOME Project*. Produced by the Canada Centre for Remote Sensing and the Canadian Forest Service, Natural Resources Canada. On CD-ROM from the Canada Centre for Remote Sensing, Ottawa, Ontario.
- Cihlar, J., Latifovic, R., Beaubien, J., Guindon, B., & Palmer, M. (2002). A TM-based accuracy assessment of land cover product for Canada derived from SPOT4/VGT data. *Canadian Journal of Remote Sensing*, (accepted for publication).
- Cohen, J. (1960). A coefficient of agreement for nominal scales. *Educational and Psychological Measurement*, 20, 37–46.
- Eidenshink, J. C., & Faundeen, J. L. (2001). The 1-km AVHRR global land data set: first stages in implementation. URL: <http://edcdaac.usgs.gov/1KM/paper.html#proc2>.
- Friedl, M. A. (1996). Examining the effects of sensor resolution and sub-pixel heterogeneity on spectral vegetation indices: implications for biophysical modeling. In D. A. Quattrochi, & M. F. Goodchild (Eds.), *Scaling of Remote Sensing Data for GIS* (pp. 113–139). New York: Lewis.
- Germogenova, T. A. (1986). *The Local Properties of the Solution of the Transport Equation*. Moscow: Nauka (in Russian).
- Gregoire, C., & Raffy, M. (1994). A spatialized APAR for heterogeneous pixels. *International Journal of Remote Sensing*, 15(12), 2393–2401.
- Hall, F. G., Huemmrich, K. F., Goetz, S. J., Sellers, P. J., & Nickeson, J. E. (1992). Satellite remote sensing of surface energy balance: success, failures, unresolved issues in FIFE. *Journal of Geophysical Research*, 97(D17), 19061–19089.
- Hansen, M., Defries, R., Townshend, J., & Sohlberg, R. (2000). Global land cover classification at 1 km spatial resolution using a classification tree approach. *International Journal of Remote Sensing*, 21, 1331–1364.
- Hu, Z., & Islam, S. (1997). A framework for analyzing and designing scale invariant remote sensing algorithms. *IEEE Transactions on Geoscience Remote Sensing*, 35(3), 747–755.
- Ioltukhovski, A. A. (1999). Radiative transfer over the surface with an arbitrary reflection: Green's functions method. *Transport Theory and Statistical Physics*, 28(4), 349–368.
- Knyazikhin, Y., & Marshak, A. (1991). Fundamental equations of radiative transfer in leaf canopies and iterative methods for their solution. In: R. B. Myneni, & J. Ross (Eds.), *Photon-Vegetation Interactions: Applications in Plant Physiology and Optical Remote Sensing* (pp. 9–43). New York: Springer-Verlag.
- Knyazikhin, Y., & Marshak, A. (2000). Mathematical aspects of BRDF modelling: adjoint problem and Green's function. *Remote Sensing Reviews*, 18, 263–280.
- Knyazikhin, Y., Marshak, A., & Myneni, R. B. (1992). Interaction of photons in a canopy of finite dimensional leaves. *Remote Sensing of Environment*, 39, 61–74.
- Knyazikhin, Y., Martonchik, J. V., Diner, D. J., Myneni, R. B., Verstraete, M. M., Pinty, B., & Gobron, N. (1998). Estimation of vegetation canopy leaf area index and fraction of absorbed photosynthetically active radiation from atmosphere-corrected MISR data. *Journal of Geophysical Research*, 103, 32239–32256.
- Knyazikhin, Y., Martonchik, J. V., Myneni, R. B., Diner, D. J., & Running, S. W. (1998). Synergistic algorithm for estimating vegetation canopy leaf area index and fraction of absorbed photosynthetically active radiation from MODIS and MISR data. *Journal of Geophysical Research*, 103, 32257–32275.
- Knyazikhin, Y., Miessen, G., Panferov, O., & Gravenhorst, G. (1997). Small-scale study of three-dimensional distribution of photosynthetically active radiation in a forest. *Agricultural and Forest Meteorology*, 88, 215–239.
- Kuus, A. (1985). The hot-spot effect of a uniform vegetative cover. *Soviet Journal of Remote Sensing*, 3, 645–658.
- Li, X., & Strahler, A. H. (1992). Geometrical-optical bidirectional reflectance modeling of the discrete crown vegetation canopy: effect of crown shape and mutual shadowing. *IEEE Transactions on Geoscience Remote Sensing*, 30, 276–292.
- Lotsch, A., Tian, Y., Friedl, M. A., & Myneni, R. B. (2002). Land cover mapping in support of LAI/FPAR retrievals from EOS-MODIS and MISR: classification methods and sensitivities to errors. *International Journal of Remote Sensing*, (accepted for publication).
- Loveland, T. R., Merchant, J. W., Brown, J. F., Ohlen, D. O., Reed, B. C., Olsen, P., & Hutchinson, J. (1995). Seasonal land cover of the United

- States. *Annals of the Association of American Geographers*, 85 (2), 339–399.
- Marshak, A. (1989). Effect of the hot spot on the transport equation in plant canopies. *Journal of Quantitative Spectroscopy & Radiative Transfer*, 42, 615–630.
- Myneni, R. B. (1991). Modeling radiative transfer and photosynthesis in three-dimensional vegetation canopies. *Agricultural and Forest Meteorology*, 55, 323–344.
- Myneni, R. B., Marshak, A., & Knyazikhin, Y. (1991). Transport theory for a leaf canopy of finite dimensional scattering centers. *Journal of Quantitative Spectroscopy & Radiative Transfer*, 46, 259–280.
- Myneni, R. B., Nemani, R. R., & Running, S. W. (1997). Estimation of global Leaf Area Index and Absorbed Par using radiative transfer models. *IEEE Transactions on Geoscience Remote Sensing*, 35, 1380–1393.
- Myneni, R. B., Tucker, C. J., Asrar, G., & Keeling, C. D. (1998). Inter-annual variations in satellite-sensed vegetation index data from 1981 to 1991. *Journal of Geophysical Research*, 103(D6), 6145–6160.
- Nelson, R., & Holben, B. (1986). Identifying deforestation in Brazil using multiresolution satellite data. *International Journal of Remote Sensing*, 7(3), 429–448.
- Nilson, T. (1991). Approximate analytical methods for calculating the reflection functions of leaf canopies in remote sensing application. In: R. B. Myneni, & J. Ross (Eds.), *Photon–Vegetation Interactions: Applications in Plant Physiology and Optical Remote Sensing* (pp. 161–190). New York: Springer-Verlag.
- Panferov, O., Knyazikhin, Y., Myneni, R. B., Szarzynski, J., Engwald, S., Schnitzler, K. G., & Gravenhorst, G. (2001). The role of canopy structure in the spectral variation of transmission and absorption of solar radiation in vegetation canopies. *IEEE Transactions on Geoscience Remote Sensing*, 39(2), 241–253.
- Raffy, M. (1994). Heterogeneity and change of scale in models of remote sensing. Spatialization of multispectral models. *International Journal of Remote Sensing*, 15, 2359–2380.
- Richtmyer, R. D. (1978). *Principles of Advanced Mathematical Physics*, vol. 1, (p. 422). New York: Springer-Verlag.
- Ross, J. (1981). *The Radiation Regime and Architecture of Plant Stands* (p. 391). Norwell, MA: Dr. W. Junk.
- Running, S. W., Collatz, G. J., Washburne, J., Sorooshian, S., Dunne, T., Dickinson, R. E., Shuttleworth, W. J., Vorosmarty, C. J., & Wood, E. F. (1999). Land ecosystems and hydrology. In: M. D. King (Ed.), *EOS Science Plan* (pp. 197–259). Greenbelt: National Aeronautics and Space Administration.
- Sellers, P. J., Dickinson, R. E., Randall, D. A., Betts, A. K., Hall, F. G., Berry, J. A., Collatz, G. J., Denning, A. S., Mooney, H. A., Nobre, C. A., Sato, N., Field, C. B., & Henderson-Sellers, A. (1997). Modeling the exchanges of energy, water, carbon between continents and the atmosphere. *Science*, 275, 502–509.
- Stamnes, K. (1982). Reflection and transmission by a vertically inhomogeneous planetary atmosphere. *Planetary and Space Science*, 30, 727–732.
- Tian, Y., Zhang, Y., Knyazikhin, Y., Myneni, R. B., Glassy, J. M., Dedieu, D., & Running, S. W. (2000). Prototyping of MODIS LAI and FPAR algorithm with LASUR and LANDSAT data. *IEEE Transactions on Geoscience Remote Sensing*, 38(5), 2387–2401.
- Titov, G. A. (1998). Radiative horizontal transport and absorption in strato-cumulus clouds. *Journal of the Atmospheric Sciences*, 55, 2549–2560.
- Townshend, J. R. G., & Justice, C. O. (1988). Selecting the spatial resolution of satellite sensors required for global monitoring of land transformations. *International Journal of Remote Sensing*, 9, 187–236.
- Van de Hulst, H. C. (1981). *Light Scattering by Small Particles* (p. 470). New York: Dover Publications.
- Verstraete, M. M., Pinty, B., & Dickinson, R. E. (1990). A physical model of the bidirectional reflectance of vegetation canopies: 1. Theory. *Journal of Geophysical Research*, 95, 11765–11775.
- Vladimirov, V. S. (1963). Mathematical problems in the one-velocity theory of particle transport. Tech. Rep. AECL-1661, At. Energy of Can., Chalk River, Ontario.
- Wang, Y., Tian, Y., Zhang, Y., El-Saleous, N., Knyazikhin, Y., Vermote, E., & Myneni, R. B. (2001). Investigation of product accuracy as a function of input and model uncertainties: case study with SeaWiFS and MODIS LAI/FPAR algorithm. *Remote Sensing of Environment*, 78, 296–311.
- Weiss, M., Baret, F., Myneni, R. B., Pragnere, A., & Knyazikhin, Y. (2000). Investigation of a model inversion technique to estimate canopy biophysical variables from spectral and directional reflectance data. *Agronomie*, 20, 3–22.
- Woodcock, C. E., & Strahler, A. H. (1987). The factor of scale in remote sensing. *Remote Sensing of Environment*, 21, 311–332.
- Zhang, Y., Shabanov, N., Knyazikhin, Y., & Myneni, R. B. (2002). Assessing the information content of multiangle satellite data for mapping biomes: II. Theory. *Remote Sensing of Environment*, 80, 435–446.
- Zhang, Y., Tian, Y., Knyazikhin, Y., Martonchik, J. V., Diner, D. J., Leroy, M., & Myneni, R. B. (2000). Prototyping of MISR LAI and FPAR algorithm with POLDER data over Africa. *IEEE Transactions on Geoscience Remote Sensing*, 38(5), 2402–2418.